

Two-spinon dynamic structure factor of the one-dimensional $S=1/2$ Heisenberg Antiferromagnet

Michael Karbach and Gerhard Müller

Department of Physics, The University of Rhode Island, Kingston RI 02881-0817

A. Hamid Bougourzi

Institute of Theoretical Physics, SUNY at Stony Brook, Stony Brook, NY 11794

(September 3, 2018)

The exact expression derived by Bougourzi, Couture, and Kacir for the 2-spinon contribution to the dynamic spin structure factor $S_{zz}(q, \omega)$ of the one-dimensional $S=1/2$ Heisenberg antiferromagnet at $T = 0$ is evaluated for direct comparison with finite-chain transition rates ($N \leq 28$) and an approximate analytical result previously inferred from finite- N data, sum rules, and Bethe-ansatz calculations. The 2-spinon excitations account for 72.89% of the total intensity in $S_{zz}(q, \omega)$. The singularity structure of the exact result is determined analytically and its spectral-weight distribution evaluated numerically over the entire range of the 2-spinon continuum. The leading singularities of the frequency-dependent spin autocorrelation function, static spin structure factor, and q -dependent susceptibility are determined via sum rules.

I. INTRODUCTION

Notwithstanding the fact that Bethe¹ found the key that solves the one-dimensional (1D) $S=1/2$ Heisenberg model,

$$H = J \sum_{l=1}^N \mathbf{S}_l \cdot \mathbf{S}_{l+1}, \quad (1.1)$$

as early as 1931, the emergence of explicit results for various physical quantities (ground-state energy,² excitation spectrum,³ magnetization curve, susceptibility,^{4,5} thermodynamics⁶) was slow at first and then faster since around 1960. Interest in this model began to spread far and wide when the first compounds with quasi-1D magnetic properties were synthesized and investigated experimentally.

However, the dynamics of the 1D Heisenberg antiferromagnet, i.e. Hamiltonian (1.1) with $J > 0$, has remained elusive to any rigorous approach during all those years. An exact result for the dynamic spin structure factor

$$S_{zz}(q, \omega) \equiv \frac{1}{N} \sum_{l,n} e^{iqn} \int_{-\infty}^{+\infty} dt e^{i\omega t} \langle S_l^z(t) S_{l+n}^z \rangle, \quad (1.2)$$

in particular, would have been of great value for the interpretation of a host of experimental data.⁷

Significant progress in the understanding of the $T = 0$ dynamics resulted from the observation⁸ that almost all

the spectral weight in $S_{zz}(q, \omega)$ is carried by a special class of Bethe-ansatz solutions with excitation energies (in units of J henceforth)

$$\omega_m(q) = \pi \sin \frac{q}{2} \cos \left(\frac{q}{2} - \frac{q_m}{2} \right) \quad (1.3)$$

for $N \rightarrow \infty$, $0 \leq q \leq \pi$, $0 \leq q_m \leq q$. They form a two-parameter continuum in the (q, ω) -plane bounded by the branches

$$\omega_L(q) = \frac{\pi}{2} \sin q, \quad \omega_U(q) = \pi \sin \frac{q}{2}. \quad (1.4)$$

These excitations were later named *2-spinon* states. Their density of states (after rescaling by a factor $2\pi/N$) is:⁸

$$D(q, \omega) = \frac{\Theta(\omega - \omega_L(q)) \Theta(\omega_U(q) - \omega)}{\sqrt{\omega_U^2(q) - \omega^2}}. \quad (1.5)$$

The $T = 0$ dynamic spin structure factor for a finite system with even N and periodic boundary conditions can be written in the form

$$S_{zz}(q, \omega) = 2\pi \sum_{\lambda} M_{\lambda} \delta(\omega - \omega_{\lambda}), \quad (1.6)$$

where $M_{\lambda} = |\langle G | S_q^z | \lambda \rangle|^2$ with $S_q^z = N^{-1/2} \sum_l e^{iql} S_l^z$ are the transition rates between the singlet ($S_T = 0$) ground state $|G\rangle$ and the triplet ($S_T = 1$) states $|\lambda\rangle$ with finite- N excitation energies ω_{λ} . Among them are the $N(N+2)/8$ 2-spinon excitations, which contribute most of the spectral weight.

The finite-chain analysis of Ref. 8 suggested that the scaled transition rates NM_{λ} vary smoothly with q and ω . The consequence could be that the exact 2-spinon part of the dynamic structure factor is expressible, in the limit $N \rightarrow \infty$, as a product

$$S_{zz}^{(2)}(q, \omega) = M(q, \omega) D(q, \omega), \quad (1.7)$$

with a smooth transition-rate function $M(q, \omega)$, toward which the scaled finite- N transition rates converge. This scenario is indeed realized in the related XX model,^{9,10} where the 2-spinon density of states is given by (1.5) with modified spectral boundaries, and the transition-rate function is a constant.⁸

II. APPROXIMATE TRANSITION RATES

In the Heisenberg model (1.1), the finite- N data for the 2-spinon matrix elements indicate that $M(q, \omega)$ diverges at $\omega = \omega_L(q)$ and vanishes at $\omega = \omega_U(q)$. In Ref. 8 the expression

$$M^{(a)}(q, \omega) = \sqrt{\frac{\omega_U^2(q) - \omega^2}{\omega^2 - \omega_L^2(q)}} \quad (2.1)$$

for the 2-spinon transition-rate function was proposed on the basis of this observation and the following three requirements: The resulting (approximate) 2-spinon dynamic structure factor $S_{zz}^{(a)}(q, \omega) = M^{(a)}(q, \omega)D(q, \omega)$ must produce, for $q = \pi$, the correct infrared exponent.^{11,12} Furthermore, it must produce the correct q -dependence of the known first frequency moment,^{8,13}

$$K_1(q) \equiv \int_0^\infty \frac{d\omega}{2\pi} \omega S_{zz}(q, \omega) = -\frac{2E_G}{3N}(1 - \cos q), \quad (2.2)$$

where $E_G = -N(\ln 2 - 1/4)$ is the ground-state energy,² and, via the sum rule

$$\chi(q) \equiv \frac{1}{\pi} \int_0^\infty \frac{d\omega}{\omega} S_{zz}(q, \omega), \quad (2.3)$$

the correct value for the direct susceptibility:^{4,5} $\chi(0) = 1/\pi^2$. The resulting approximate expression,¹⁴

$$S_{zz}^{(a)}(q, \omega) = \frac{\Theta(\omega - \omega_L(q))\Theta(\omega_U(q) - \omega)}{\sqrt{\omega^2 - \omega_L^2(q)}}, \quad (2.4)$$

for the 2-spinon dynamic structure factor has been used quite frequently for the interpretation of inelastic neutron scattering measurements on a number of quasi-1D antiferromagnets at low temperature,⁷ and for comparisons with the results of various computational studies.^{15–17}

It is interesting to note in this context that the exact dynamic structure factor $S_{zz}(q, \omega)$ of the Haldane-Shastry model has a structure very similar to (2.4).¹⁸ In that model, as in the XX model, all the spectral weight of $S_{zz}(q, \omega)$ is carried by the 2-spinon excitations.

III. EXACT TRANSITION RATES

A detailed assessment of the merits and limitations of the result (2.4) has become possible only recently through a remarkable new development. By approaches based on the concept of infinite-dimensional symmetries which had been developed in the context of string theory, conformal field theory, and quantum groups¹⁹ Bougourzi, Couture, and Kacir²⁰ were able to derive the exact expression for the 2-spinon transition-rate function in the form²¹

$$M(q, \omega) = \frac{1}{2} e^{-I(t)} \quad (3.1)$$

where $t = 2(\beta_1 - \beta_2)/\pi$ and

$$I(t) = \int_0^\infty dx \frac{\cosh(2x) \cos(xt) - 1}{x \sinh(2x) \cosh x} e^x, \quad (3.2)$$

$$\omega = \frac{\pi}{2 \cosh \beta_1} + \frac{\pi}{2 \cosh \beta_2}, \quad (3.3a)$$

$$q = -\cot^{-1}(\sinh \beta_1) - \cot^{-1}(\sinh \beta_2). \quad (3.3b)$$

By solving Eqs. (3.3) we can express the auxiliary variable t as a function of the two physical variables q, ω :

$$t = \frac{4}{\pi} \cosh^{-1} \sqrt{\frac{\omega_U^2(q) - \omega_L^2(q)}{\omega^2 - \omega_L^2(q)}}. \quad (3.4)$$

For the numerical evaluation of (3.1) we separate the singular part from the integral (3.2):

$$I(t) = -I_0 - \ln \left(t \sinh^2 \frac{\pi t}{4} \right) + h(t), \quad (3.5)$$

where

$$h(t) = \text{Ci}(t) + f_1(t) - f_2(t), \quad (3.6a)$$

$$f_1(t) = \int_1^\infty \frac{dx}{x} \frac{\cos(xt)}{\cosh^2 x}, \quad f_2(t) = \int_0^1 \frac{dx}{x} \frac{\cos(xt)}{\coth^2 x}, \quad (3.6b)$$

$$I_0 = \gamma + f_1(0) - f_2(0) = 0.3677103\dots \quad (3.6c)$$

A series expansion of $s(t) \equiv [\ln t + C - h(t)]/2$,

$$s(t) = \int_0^\infty dx \frac{\sin^2(xt/2)}{x \cosh^2 x} = \sum_{m=1}^\infty (-1)^m m \ln \left(1 + \frac{t^2}{4m^2} \right),$$

$$C \equiv e^{I_0}/2 = 0.72221\dots, \quad (3.7)$$

brings (3.1) with t from (3.4) into closed form:

$$M(q, \omega) = Ct \sinh \left(\frac{\pi t}{4} \right) \times \prod_{m=1}^\infty \frac{\{1 + [t/(4m-2)]^2\}^{2m-1}}{\{1 + [t/4m]^2\}^{2m}}. \quad (3.8)$$

The exact 2-spinon part of $S_{zz}(q, \omega)$, i.e. the function (1.7) with the density of states (1.5) and the transition-rate function (3.1) evaluated numerically via (3.5) with (3.4) is plotted in Fig. 1(a). For comparison, the approximate result (2.4) is shown in Fig. 1(b). The two results look very similar, yet there are subtle differences, which may not matter for most experimental comparisons but

are important for comparisons with other theoretical results.

Both expressions diverge at the lower spectral boundary $\omega_L(q)$. At the upper boundary $\omega_U(q)$, $S_{zz}^{(a)}(q, \omega)$ has discontinuity, whereas $S_{zz}^{(2)}(q, \omega)$ approaches zero continuously over a rounded shoulder.

The structure of the exact transition rate function (3.1) lends itself naturally to be factorized into the approximate function (2.1) and a correction which accounts for the modified singularities at the boundaries of the 2-spinon continuum:

$$M(q, \omega) = M^{(a)}(q, \omega) \sqrt{Ct/2} e^{h(t)/2}. \quad (3.9)$$

IV. SINGULARITIES AT $\omega_L(q)$ AND $\omega_U(q)$

What is the precise nature of the leading singularity in the transition-rate function $M(q, \omega)$ and in the 2-spinon dynamic structure factor $S_{zz}^{(2)}(q, \omega)$ at the spectral boundaries $\omega_U(q)$ and $\omega_L(q)$, and how do these singularities compare with those of the approximate results $S_{zz}^{(a)}(q, \omega)$ and $M^{(a)}(q, \omega)$? The answer is obtained by inserting (3.5) into (3.1), evaluating the leading term for $t \rightarrow 0$ and $t \rightarrow \infty$, respectively, and inserting (3.4) expanded accordingly.

At $\omega_U(q)$ the transition-rate function is thus found to approach zero linearly,

$$M(q, \omega) \xrightarrow{\omega \rightarrow \omega_U} \frac{8C}{\pi} \frac{\omega_U(q)}{\omega_U^2(q) - \omega_L^2(q)} [\omega_U(q) - \omega], \quad (4.1)$$

which implies that the 2-spinon dynamic structure factor vanishes in a square-root cusp:

$$S_{zz}^{(2)}(q, \omega) \xrightarrow{\omega \rightarrow \omega_U} \frac{8C}{\pi} \frac{\sqrt{2\omega_U(q)}}{\omega_U^2(q) - \omega_L^2(q)} \sqrt{\omega_U(q) - \omega}. \quad (4.2)$$

$M^{(a)}(q, \omega)$ vanishes more slowly, $\sim [\omega_U(q) - \omega]^{1/2}$, implying that $S_{zz}^{(a)}(q, \omega)$ drops to zero abruptly.

At $\omega_L(q)$ we find a square-root divergence (for $q \neq \pi$) in both the exact and the approximate transition-rate functions, but in the former this power-law singularity is accompanied by a logarithmic correction:

$$M(q, \omega) \xrightarrow{\omega \rightarrow \omega_L} \frac{\sqrt{C/2}}{\pi} \sqrt{\frac{\omega_U^2(q) - \omega_L^2(q)}{\omega_L(q)}} \times \frac{1}{\sqrt{\omega - \omega_L(q)}} \sqrt{\ln \frac{1}{\omega - \omega_L(q)}}. \quad (4.3)$$

Since the 2-spinon density of states is a step function near $\omega_L(q)$, only the prefactor changes in $S_{zz}^{(2)}(q, \omega)$:

$$S_{zz}^{(2)}(q, \omega) \xrightarrow{\omega \rightarrow \omega_L} \frac{M(q, \omega)}{\sqrt{\omega^2(q) - \omega_L^2(q)}}. \quad (4.4)$$

For $q \rightarrow \pi$ the singularity at $\omega_L(q)$ turns into a much stronger infrared singularity:

$$M(\pi, \omega) \xrightarrow{\omega \rightarrow 0} \sqrt{2\pi C} \frac{1}{\omega} \sqrt{\ln \frac{1}{\omega}}, \quad (4.5)$$

$$S_{zz}^{(2)}(\pi, \omega) \xrightarrow{\omega \rightarrow 0} \sqrt{\frac{2C}{\pi}} \frac{1}{\omega} \sqrt{\ln \frac{1}{\omega}}. \quad (4.6)$$

V. SPIN AUTOCORRELATION FUNCTION

A quantity of some interest in various experimental and theoretical contexts is the frequency-dependent spin autocorrelation function

$$\Phi_{zz}(\omega) \equiv \int_{-\infty}^{+\infty} dt e^{-i\omega t} \langle S_L^z(t) S_L^z \rangle. \quad (5.1)$$

The 2-spinon contribution to $\Phi_{zz}(\omega)$,

$$\Phi_{zz}^{(2)}(\omega) \equiv \frac{1}{\pi} \int_0^\pi dq S_{zz}^{(2)}(q, \omega), \quad (5.2)$$

is a piecewise smooth function over the range of 2-spinon energies $0 < \omega < \pi$ and has singularities at $\omega = 0, \pi/2, \pi$. The approximate 2-spinon autocorrelation function inferred from (2.4) can be evaluated in terms of elliptic integrals. It has a step discontinuity at $\omega = 0$,

$$\Phi_{zz}^{(a)}(\omega) \xrightarrow{\omega \rightarrow 0} \frac{1}{\pi} + O(\omega), \quad (5.3)$$

a logarithmic divergence at $\omega = \pi/2$,

$$\Phi_{zz}^{(a)}(\omega) \xrightarrow{\omega \rightarrow \pi/2} \propto \ln \frac{1}{|\pi/2 - \omega|}, \quad (5.4)$$

and a square-root cusp at $\omega = \pi$,

$$\Phi_{zz}^{(a)}(\omega) \xrightarrow{\omega \rightarrow \pi} \propto \sqrt{\pi - \omega}. \quad (5.5)$$

The exact 2-spinon expression has logarithmic divergences at $\omega = 0, \pi/2$, and a linear cusp at $\omega = \pi$:

$$\Phi_{zz}^{(2)}(\omega) \xrightarrow{\omega \rightarrow 0} \propto \ln \frac{1}{\omega}. \quad (5.6)$$

$$\Phi_{zz}^{(2)}(\omega) \xrightarrow{\omega \rightarrow \pi/2} \propto \left(\ln \frac{1}{|\pi/2 - \omega|} \right)^{3/2}, \quad (5.7)$$

$$\Phi_{zz}^{(2)}(\omega) \xrightarrow{\omega \rightarrow \pi} \propto (\pi - \omega) \quad (5.8)$$

The functions $\Phi_{zz}^{(2)}(\omega)$ and $\Phi_{zz}^{(a)}(\omega)$ are plotted in Fig. 2.

VI. SUM RULES

How important is the 2-spinon contribution to $S_{zz}(q, \omega)$ in relation to that of other excited states? The key to the answer is provided by sum rules, such as the first frequency moment (2.2), which is known for all q , or the susceptibility (2.3), which is known for $q = 0$ only, or the integrated intensity (static structure factor),

$$I(q) \equiv \int_0^\infty \frac{d\omega}{2\pi} S_{zz}(q, \omega), \quad (6.1)$$

of which we know the grand total:

$$I_T = \frac{1}{\pi} \int_0^\pi dq I(q) = \langle (S_i^z)^2 \rangle = \frac{1}{4}. \quad (6.2)$$

The exact 2-spinon contribution to the n^{th} frequency moment of $S_{zz}(q, \omega)$,

$$K_n(q) \equiv \int_0^\infty \frac{d\omega}{2\pi} \omega^n S_{zz}(q, \omega), \quad (6.3)$$

as obtained from (1.7) with (1.5) and (3.1) can be brought into the form

$$K_n^{(2)}(q) = \frac{2C}{\pi^3} [\omega_U(q)]^{n+1} k_n(q), \quad (6.4)$$

where

$$k_n(q) = \int_0^\infty dx \frac{x \sinh x}{\cosh^2 x} \left(1 - \sin^2 \frac{q}{2} \tanh^2 x\right)^{\frac{n-1}{2}} e^{-s(4x/\pi)}. \quad (6.5)$$

For $n = 2m + 1 = 1, 3, \dots$ this expression reduces to a polynomial in $\cos q$,

$$K_{2m+1}^{(2)}(q) = \frac{C}{\pi} \left(\frac{\pi^2}{2}\right)^m \sum_{l=0}^m \binom{m}{l} \frac{(-1)^l}{2^l} \kappa_l (1 - \cos q)^{m+1+l}, \quad (6.6a)$$

$$\kappa_l \equiv \int_0^\infty dx \frac{x (\tanh x)^{2l+1}}{\cosh x} e^{-s(4x/\pi)}. \quad (6.6b)$$

The exact sum rules for $K_{2m+1}^{(2)}(q)$ were shown to have precisely this general structure,^{22,23} which, incidentally, is also reproduced by the frequency moments $K_{2m+1}^{(a)}(q)$ of $S_{zz}^{(a)}(q, \omega)$. However, the exact coefficients of the polynomial are only known for $m = 0$. Comparison of

$$K_1^{(2)}(q) = \frac{C}{\pi} \kappa_0 (1 - \cos q), \quad \kappa_0 = 0.9163\dots, \quad (6.7)$$

with (2.2) provides one way of measuring the relative spectral weight of the 2-spinon excitations:

$$\frac{K_1^{(2)}(q)}{K_1(q)} = 0.7130\dots \quad (6.8)$$

A somewhat larger share of spectral weight, $K_1^{(a)}(q)/K_1(q) = 0.8462\dots$, is accounted for by $S_{zz}^{(a)}(q, \omega)$.

A different way of measuring the relative 2-spinon spectral weight is provided by the static structure factor (6.1). Here, the missing spectral weight of higher-lying excitations is weighted less heavily.

The exact 2-spinon static structure factor $I^{(2)}(q) = K_0^{(2)}(q)$ taken from (6.4) and integrated over q yields the total 2-spinon intensity

$$I_T^{(2)} = \frac{4C}{\pi^3} \int_0^\infty dx \frac{x^2}{\cosh x} e^{-s(4x/\pi)} \simeq 0.7289 I_T. \quad (6.9)$$

The total intensity of $S_{zz}^{(a)}(q, \omega)$ is⁸ $I_T^{(a)} \simeq 0.7424 I_T$.

The observation that $S_{zz}^{(a)}(q, \omega)$ overestimates the total 2-spinon intensity by a smaller fraction, $I_T^{(a)}/I_T^{(2)} \simeq 1.0185$, than the first frequency moment of the 2-spinon spectral weight, $K_1^{(a)}(q)/K_1^{(2)}(q) \simeq 1.1868$, is consistent with the observation made previously that it predicts too much spectral weight near $\omega_U(q)$ and too little near $\omega_L(q)$.

At small q , where the 2-spinon continuum is very narrow, all frequency moments of $S_{zz}^{(2)}(q, \omega)$ and $S_{zz}^{(a)}(q, \omega)$ have exactly the same ratio

$$\frac{K_n^{(a)}(q)}{K_n^{(2)}(q)} \xrightarrow{q \rightarrow 0} \frac{4C}{\pi} \kappa_0 = 0.8426\dots \quad (6.10)$$

The implications of the frequency moments $K_0^{(2)}(q)$ and $K_{-1}^{(2)}(q)$ for the singularities of the static structure factor and the static susceptibility, respectively, will be discussed later.

VII. FINITE-CHAIN RESULTS

To what extent and accuracy can the spectral-weight distribution of $S_{zz}(q, \omega)$ be reconstructed from (1.6) on the basis of finite-chain data for excitation energies ω_λ and transition rates M_λ ? In a generic situation, the chances for success may be remote. Convergence of the finite- N data for (1.6) toward the infinite- N spectral density may only exist in an average sense, such as can be realized, at least in principle, by a histogram representation of (1.6), but hardly in practice given the very coarse-grained spectral-weight distribution even in the largest systems that can be handled computationally.

Among the ever growing collection of Bethe-ansatz solvable models, there exist numerous situations where

the spectral density of interest is dominated by a specific class of excitations that can be identified in terms of Bethe quantum numbers. When the dynamically dominant class of excitations consists of a two-parameter continuum, as is frequently the case, the task of reconstructing that spectral density from finite- N data with reasonable accuracy may be perfectly within the reach of state-of-the-art computational applications.

In the case at hand, the 2-spinon excitation energies ω_λ can be evaluated for finite chains over a wide range of N and then again for infinite N , all via Bethe ansatz. The finite- N transition rates M_λ can be evaluated directly from the Bethe-ansatz wave function for the ground state and the 2-spinon states up to $N = 16$ and indirectly from the finite- N ground-state wave function via the recursion method¹⁷ up to $N = 28$.

The crucial point for the reconstruction of the 2-spinon part of the dynamic structure factor $S_{zz}(q, \omega)$ is that it factorizes into two smooth functions: the density of states $D(q, \omega)$, which can be determined exactly via Bethe ansatz, and the transition rate function $M(q, \omega)$, toward which the finite- N transition rates seem to converge in the following sense: pick any sequence of finite- N 2-spinon states with energies $\omega_\lambda(N)$ and wave numbers $q_\lambda(N)$ converging toward (q, ω) as $N \rightarrow \infty$. Then the associated scaled transition rates $NM_\lambda(N)$ converge toward the exact transition rate function $M(q, \omega)$.

In the main plot of Fig. 3 we show the transition rate functions $M(\pi, \omega)$ (exact, solid line) and $M^{(a)}(\pi, \omega)$ (approximate, dashed line) along with scaled finite- N transition rates NM_λ for $N = 6, 8, \dots, 28$. The downward deviation of $M^{(a)}(\pi, \omega)$ from $M(\pi, \omega)$ at low frequencies is due to the lacking logarithmic corrections in the infrared divergence and the upward deviation at high frequencies due to the different cusp singularity at $\omega_U(\pi)$.

All finite- N data points fall close to the solid line. Their deviations from that line have an irregular appearance at first sight. This is attributable to the fact that an increasing number of spectral contributions from systems with increasing N are distributed over a fixed frequency interval. However, when we focus on the lowest-lying excitation, for example, we see that the data points move away from the dashed line toward the solid line. The uniform convergence of this particular sequence of data points is best observable in the representation of the inset on the left of Fig. 3.

The region near $\omega_U(\pi)$ is shown magnified in the inset on the right. Here the finite- N data converge in a much more complicated pattern. Nevertheless, the trend is clearly toward the linear behavior of the solid line and away from the square-root behavior of the dashed line.

The corresponding results for $q = \pi/2$ are depicted in Fig. 4. Here the highest 2-spinon excitation for $N = 28$, which we were unable to compute with sufficient accuracy via the recursion method, is not included. Even with the few finite-chain data points available in this case, the finite-size scaling behavior of the transition rates M_λ and their convergence toward the exact transition-rate

function is again convincingly determined.

Given the exact asymptotic finite-size gap of the lowest 2-spinon excitation at $q = \pi$,²⁴

$$\omega_1 \xrightarrow{N \rightarrow \infty} \frac{\alpha}{N}, \quad \alpha = \frac{\pi^2}{2}, \quad (7.1)$$

and the exact infrared divergence (4.6) of $S_{zz}^{(2)}(q, \omega)$, it is possible to determine, under standard scaling assumptions, the leading N -dependence of the integrated intensity at $q = \pi$,

$$I(\pi, N) \xrightarrow{N \rightarrow \infty} \frac{m_0}{2\pi} (\ln N)^{3/2} \quad (7.2)$$

with $m_0 = \sqrt{2C/\pi}$. The exact coefficient, $m_0/2\pi = 0.1079\dots$, is significantly higher than the value 0.09052 predicted in a recent DMRG study.²⁵ The leading singularity of the integrated intensity for $N = \infty$, $q \rightarrow \pi$ is then predicted to be of the form

$$I(q, \infty) \xrightarrow{q \rightarrow \pi} \frac{m_0}{2\pi} \left[-\ln \left(1 - \frac{q}{\pi} \right) \right]^{3/2}, \quad (7.3)$$

which is consistent with the exactly known leading asymptotic term of the static spin correlation function²⁶ $\langle S_i^z S_{i+n}^z \rangle \sim (-1)^n n^{-1} (\ln n)^{1/2} / n$.

The corresponding leading terms for the static susceptibility read:

$$\chi(\pi, N) \xrightarrow{N \rightarrow \infty} \frac{m_0}{\pi\alpha} N \sqrt{N}, \quad (7.4)$$

$$\chi(q, \infty) \xrightarrow{q \rightarrow \pi} \propto \frac{\sqrt{-\ln(\pi - q)}}{\pi - q}. \quad (7.5)$$

ACKNOWLEDGMENTS

The work at URI was supported by NSF Grant DMR-93-12252, and by the Max Kade Foundation. The work at SUNYSB was supported by NSF Grant PHY-93-09888. A.H.B. would like to thank M. Couture for encouragements and stimulating discussions. Access to the computing facilities at the national Center for Supercomputing Applications, University of Illinois at Urbana-Champaign is gratefully acknowledged.

¹ H. Bethe, Z. Phys. **71**, 205 (1931).

² L. Hulthén, Arkiv Mat. Astron. Fysik A11 **26**, 1 (1938).

³ J. des Cloizeaux and J.J. Pearson, Phys. Rev. **128**, 2131 (1962).

⁴ R.B. Griffiths, Phys. Rev. **133**, A768 (1964).

⁵ C.N. Yang and C.P. Yang, Phys. Rev. **150**, 321 (1966); **150**, 327 (1966); **151**, 258 (1966).

- ⁶ M. Gaudin, Phys. Rev. Lett. **26**, 1301 (1971); M. Takahashi, Prog. Theor. Phys. **46**, 401 (1971).
- ⁷ S.E. Nagler *et al.*, Phys. Rev. B **44**, 12361 (1991); D.A. Tennant, T.G. Perring, R.A. Cowley, and S.E. Nagler, Phys. Rev. Lett. **70**, 4003 (1993); D.C. Dender *et al.*, Phys. Rev. B **53**, 2583 (1996).
- ⁸ G. Müller, H. Thomas, H. Beck, and J.C. Bonner, Phys. Rev. B **24**, 1429 (1981).
- ⁹ T. Niemeijer, Physica **36**, 377 (1966).
- ¹⁰ S. Katsura, T. Horiguchi, and M. Suzuki, Physica **46**, 67 (1970).
- ¹¹ A. Luther and I. Peschel, Phys. Rev. B **12**, 3908 (1975).
- ¹² The logarithmic corrections to the $\sim \omega^{-1}$ singularity were not known at the time.
- ¹³ P.C. Hohenberg and W.F. Brinkman, Phys. Rev. B **10**, 128 (1974).
- ¹⁴ Alternative requirements considered in Ref. 8 yield prefactors in (8) which are slightly greater than one.
- ¹⁵ S. Haas, J. Riera, and E. Dagotto, Phys. Rev. B **48**, 3281 (1993).
- ¹⁶ K. Hallberg, Phys. Rev. B **52**, R9827 (1995).
- ¹⁷ A. Fledderjohann, M. Karbach, K.-H. Mütter, and P. Wielath, J. Phys.: Condens. Matter **7**, 8993 (1995).
- ¹⁸ F.D.M. Haldane and M.R. Zirnbauer, Phys. Rev. Lett. **71**, 4055 (1993).
- ¹⁹ M. Jimbo and T. Miwa, *Algebraic Analysis of Solvable Lattice Models*, (American Mathematical Society, CBMS, 1995).
- ²⁰ A.H. Bougourzi, M. Couture, and M. Kacir, Preprint ITP-SB-96-21, Stony Brook.
- ²¹ We have found and corrected a discrepancy in chapter 10.4 of Ref. 19, which affects the constant prefactor in (3.1).
- ²² A. Fledderjohann, M. Karbach, and K.-H. Mütter, Phys. Rev. B **53**, 11543 (1996).
- ²³ G. Müller, Phys. Rev. B **26**, 1311 (1982).
- ²⁴ F. Woynarovich and H.-P. Ecker, J. Phys. A: Math. Gen. **20**, L97 (1987).
- ²⁵ K. Hallberg, P. Horsch, and G. Martínez, Phys. Rev. B **52**, R719 (1995).
- ²⁶ R.R.P. Singh, M.E. Fisher, and R. Shankar, Phys. Rev. B **39**, 2562 (1989).

FIG. 1. (a) Exact and (b) approximate 2-spinon dynamic structure factor. Both expressions are nonzero only in the shaded region of the (q, ω) -plane bounded by $\omega_L(q)$ and $\omega_U(q)$.

FIG. 2. Two-spinon part of the frequency-dependent spin autocorrelation function. The solid line represents the exact result $\Phi_{zz}^{(2)}(\omega)$ and the dashed line the approximate result $\Phi_{zz}^a(\omega)$.

FIG. 3. Two-spinon transition-rate function at $q = \pi$. The solid line represents the exact result $M(q, \omega)$ and the dashed line the approximate result $M^{(a)}(q, \omega)$. Also shown are scaled finite-chain transition rates NM_λ for all 2-spinon excitations at $q = \pi$ of systems with $N = 6, 8, \dots, 16, 28$ spins, and for lowest 2-spinon excitations also of systems with $N = 18, 20, \dots, 26$. The low-frequency and high-frequency parts are shown again in the insets with transformed scales on both axes.

FIG. 4. Two-spinon transition-rate function at $q = \pi/2$. The solid line represents the exact result $M(q, \omega)$ and the dashed line the approximate result $M^{(a)}(q, \omega)$. Also shown are scaled finite-chain transition rates NM_λ for all 2-spinon excitations at $q = \pi$ of systems with $N = 8, 12, 16, 28$ spins. The low-frequency and high-frequency parts are shown again in the insets with transformed scales on both axes.

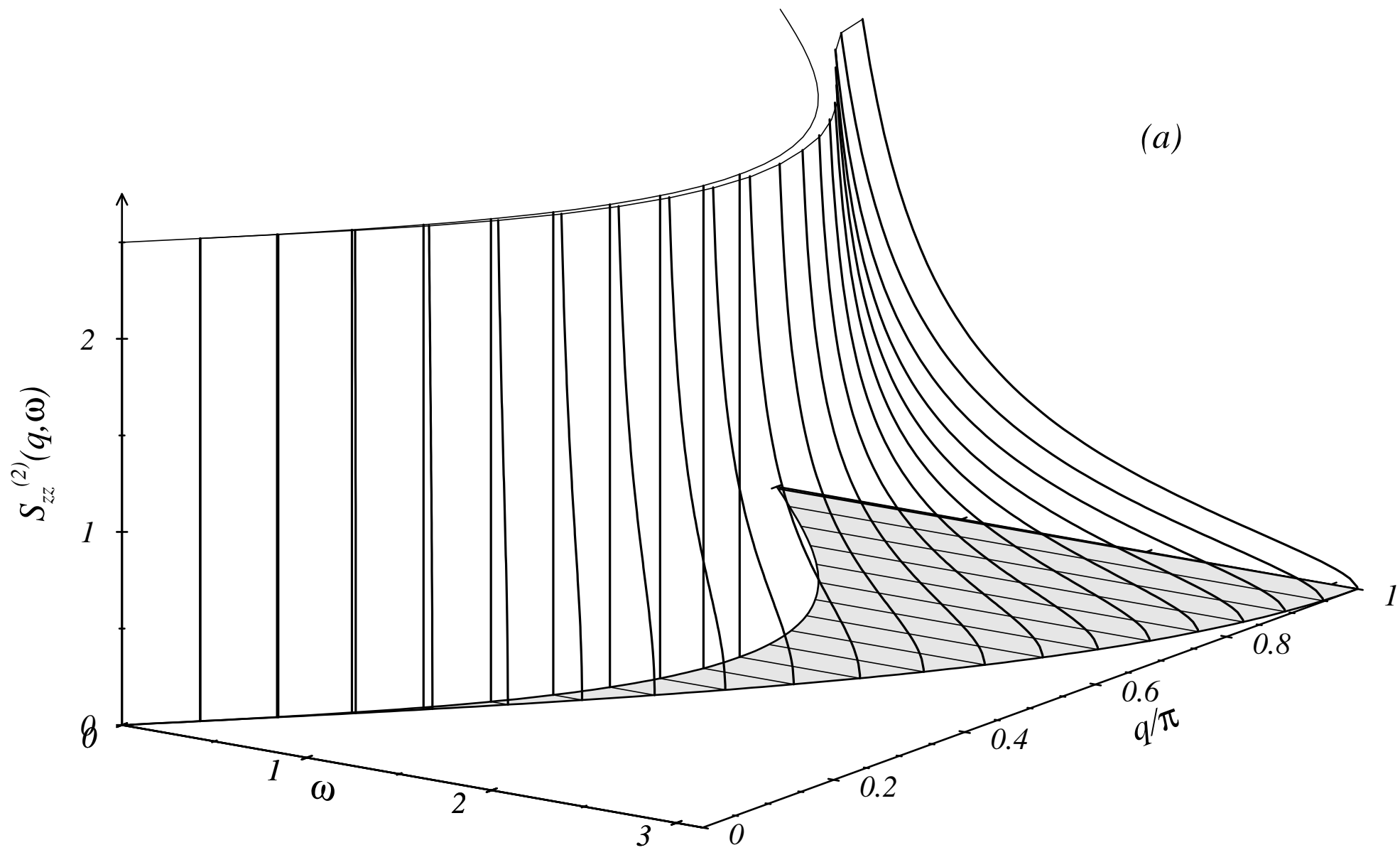


Fig. 1(a)

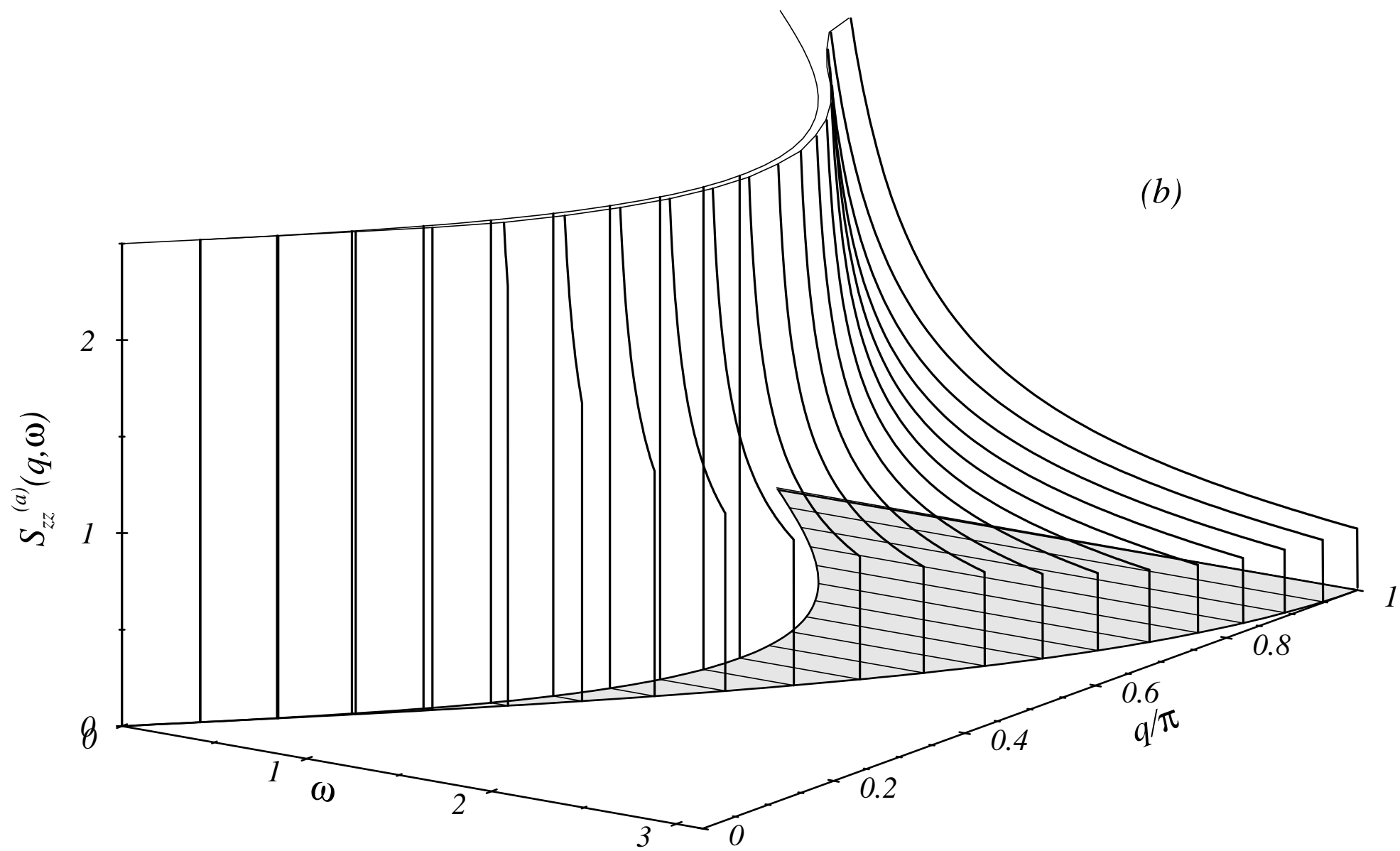


Fig. 1(b)

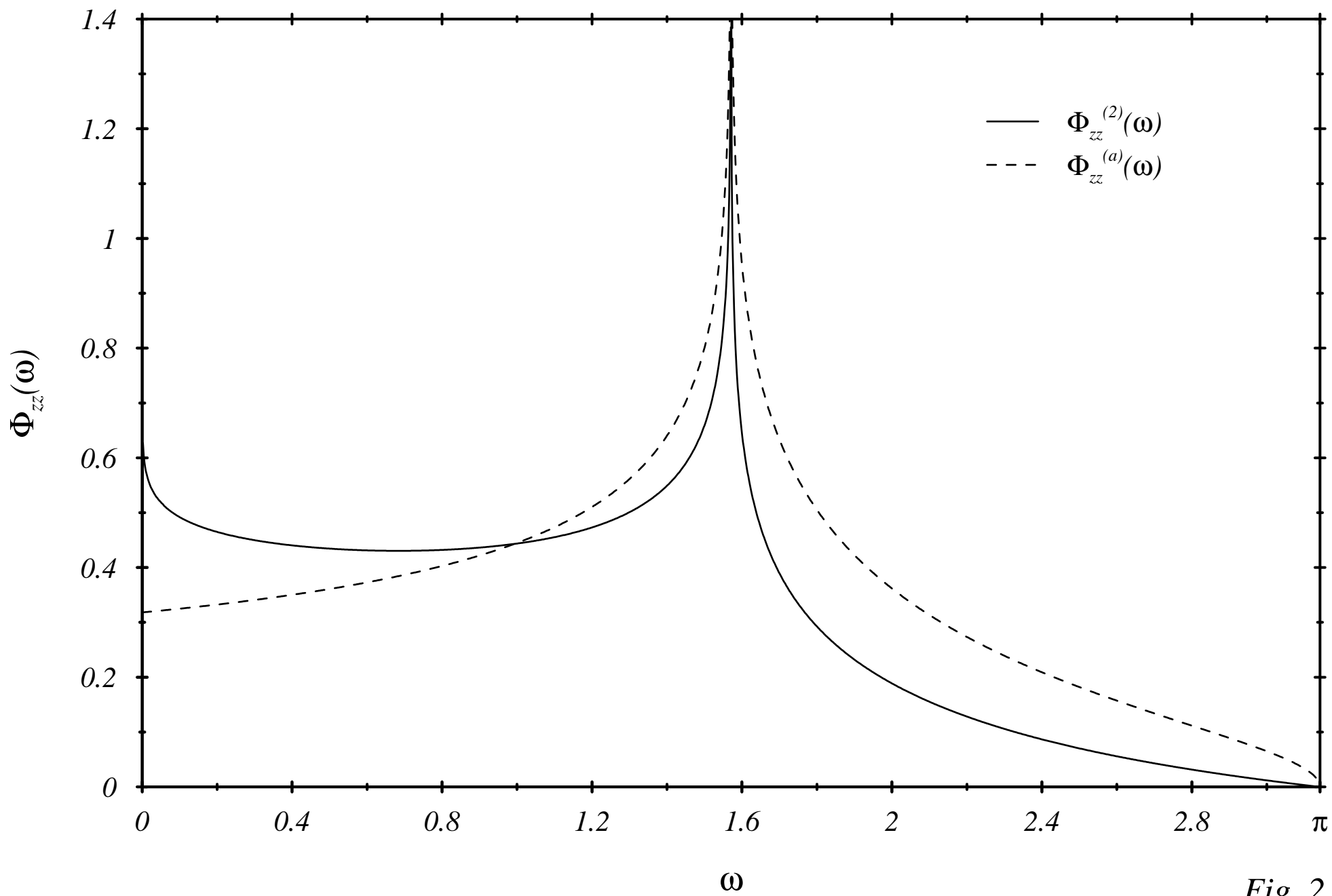


Fig. 2

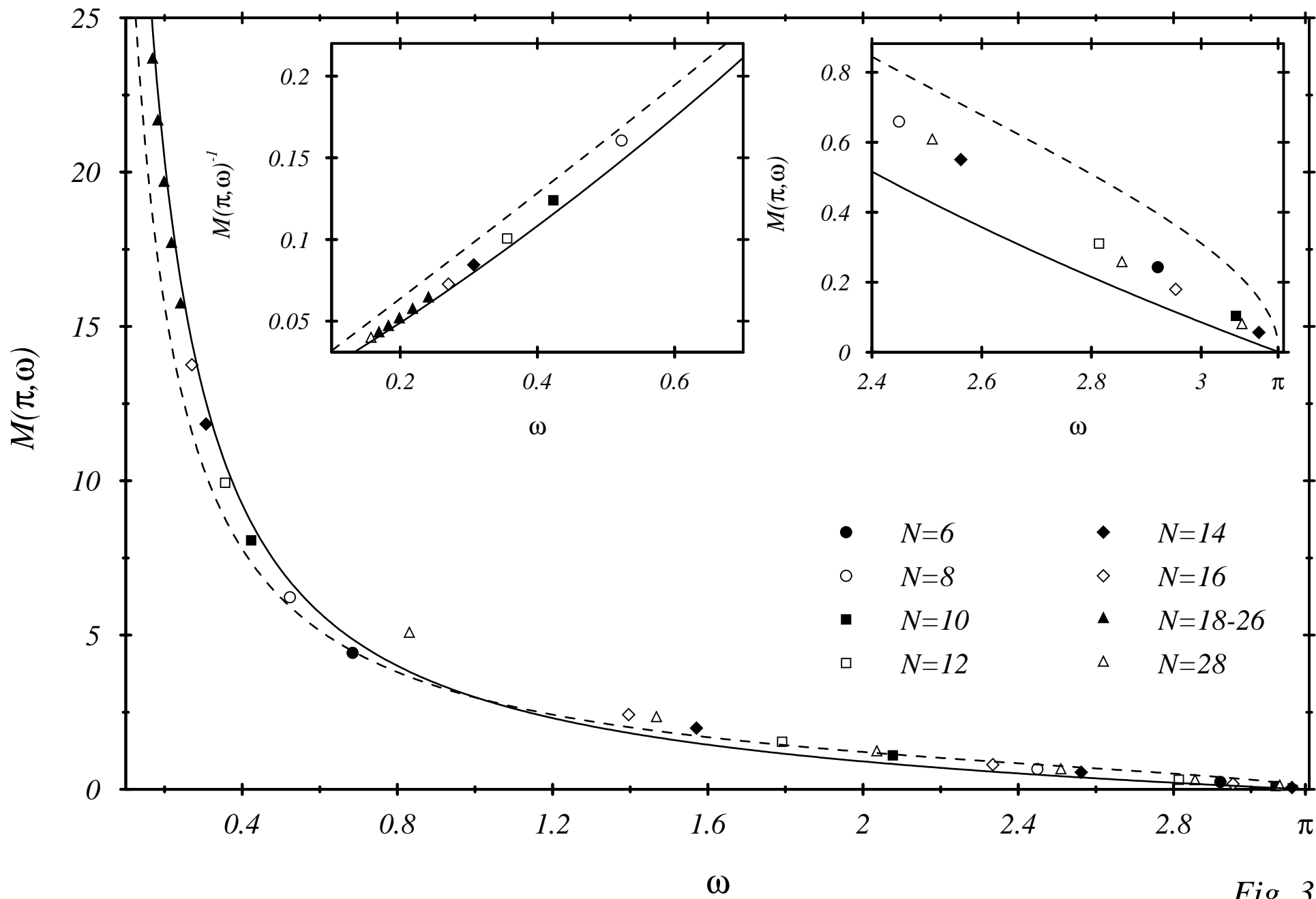


Fig. 3

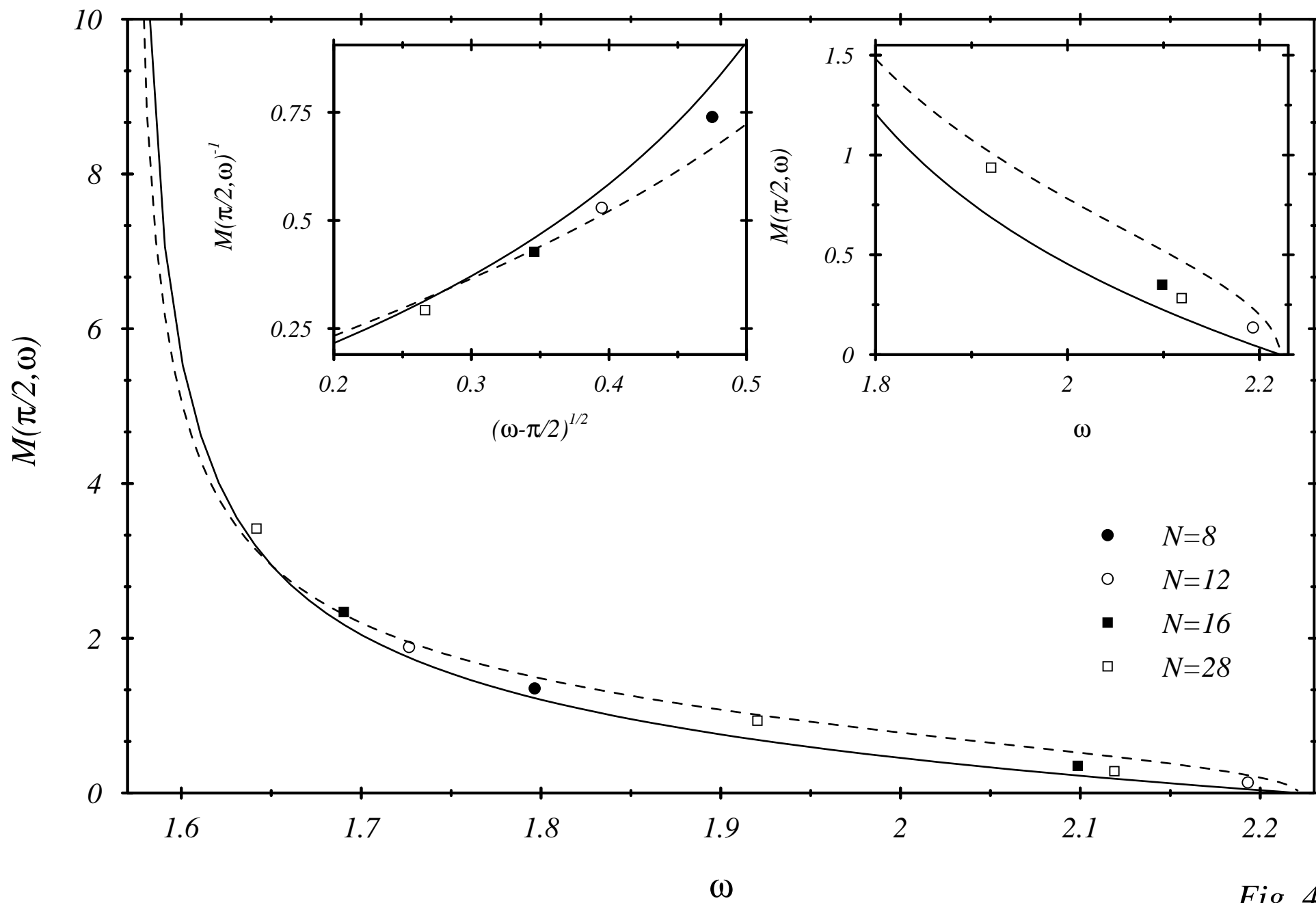


Fig. 4

Two-spinon dynamic structure factor of the one-dimensional $S=1/2$ Heisenberg Antiferromagnet

Michael Karbach and Gerhard Müller

Department of Physics, The University of Rhode Island, Kingston RI 02881-0817

A. Hamid Bougourzi

Institute of Theoretical Physics, SUNY at Stony Brook, Stony Brook, NY 11794

(August 23, 1996)

The exact expression derived by Bougourzi, Couture, and Kacir for the 2-spinon contribution to the dynamic spin structure factor $S_{zz}(q, \omega)$ of the one-dimensional $S=1/2$ Heisenberg antiferromagnet at $T = 0$ is evaluated for direct comparison with finite-chain transition rates ($N \leq 28$) and an approximate analytical result previously inferred from finite- N data, sum rules, and Bethe-ansatz calculations. The 2-spinon excitations account for 72.89% of the total intensity in $S_{zz}(q, \omega)$. The singularity structure of the exact result is determined analytically and its spectral-weight distribution evaluated numerically over the entire range of the 2-spinon continuum. The leading singularities of the frequency-dependent spin autocorrelation function, static spin structure factor, and q -dependent susceptibility are determined via sum rules.

I. INTRODUCTION

Notwithstanding the fact that Bethe¹ found the key that solves the one-dimensional (1D) $S=1/2$ Heisenberg model,

$$H = J \sum_{i=1}^N \mathbf{S}_i \cdot \mathbf{S}_{i+1}, \quad (1.1)$$

as early as 1931, the emergence of explicit results for various physical quantities (ground-state energy,² excitation spectrum,³ magnetization curve, susceptibility,^{4,5} thermodynamics⁶) was slow at first and then faster since around 1960. Interest in this model began to spread far and wide when the first compounds with quasi-1D magnetic properties were synthesized and investigated experimentally.

However, the dynamics of the 1D Heisenberg antiferromagnet, i.e. Hamiltonian (1.1) with $J > 0$, has remained elusive to any rigorous approach during all those years. An exact result for the dynamic spin structure factor

$$S_{zz}(q, \omega) \equiv \frac{1}{N} \sum_{l,n} e^{iqn} \int_{-\infty}^{+\infty} dt e^{i\omega t} \langle S_l^z(t) S_{l+n}^z \rangle, \quad (1.2)$$

in particular, would have been of great value for the interpretation of a host of experimental data.⁷

Significant progress in the understanding of the $T = 0$ dynamics resulted from the observation⁸ that almost all

the spectral weight in $S_{zz}(q, \omega)$ is carried by a special class of Bethe-ansatz solutions with excitation energies (in units of J henceforth)

$$\omega_m(q) = \pi \sin \frac{q}{2} \cos \left(\frac{q}{2} - \frac{q_m}{2} \right) \quad (1.3)$$

for $N \rightarrow \infty$, $0 \leq q \leq \pi$, $0 \leq q_m \leq q$. They form a two-parameter continuum in the (q, ω) -plane bounded by the branches

$$\omega_L(q) = \frac{\pi}{2} \sin q, \quad \omega_U(q) = \pi \sin \frac{q}{2}. \quad (1.4)$$

These excitations were later named *2-spinon* states. Their density of states (after rescaling by a factor $2\pi/N$) is:⁸

$$D(q, \omega) = \frac{\Theta(\omega - \omega_L(q)) \Theta(\omega_U(q) - \omega)}{\sqrt{\omega_U^2(q) - \omega^2}}. \quad (1.5)$$

The $T = 0$ dynamic spin structure factor for a finite system with even N and periodic boundary conditions can be written in the form

$$S_{zz}(q, \omega) = 2\pi \sum_{\lambda} M_{\lambda} \delta(\omega - \omega_{\lambda}), \quad (1.6)$$

where $M_{\lambda} = |\langle G | S_q^z | \lambda \rangle|^2$ with $S_q^z = N^{-1/2} \sum_i e^{iqi} S_i^z$ are the transition rates between the singlet ($S_T = 0$) ground state $|G\rangle$ and the triplet ($S_T = 1$) states $|\lambda\rangle$ with finite- N excitation energies ω_{λ} . Among them are the $N(N+2)/8$ 2-spinon excitations, which contribute most of the spectral weight.

The finite-chain analysis of Ref. 8 suggested that the scaled transition rates $N M_{\lambda}$ vary smoothly with q and ω . The consequence could be that the exact 2-spinon part of the dynamic structure factor is expressible, in the limit $N \rightarrow \infty$, as a product

$$S_{zz}^{(2)}(q, \omega) = M(q, \omega) D(q, \omega), \quad (1.7)$$

with a smooth transition-rate function $M(q, \omega)$, toward which the scaled finite- N transition rates converge. This scenario is indeed realized in the related XX model,^{9,10} where the 2-spinon density of states is given by (1.5) with modified spectral boundaries, and the transition-rate function is a constant.⁸

II. APPROXIMATE TRANSITION RATES

In the Heisenberg model (1.1), the finite- N data for the 2-spinon matrix elements indicate that $M(q, \omega)$ diverges at $\omega = \omega_L(q)$ and vanishes at $\omega = \omega_U(q)$. In Ref. 8 the expression

$$M^{(a)}(q, \omega) = \sqrt{\frac{\omega_U^2(q) - \omega^2}{\omega^2 - \omega_L^2(q)}} \quad (2.1)$$

for the 2-spinon transition-rate function was proposed on the basis of this observation and the following three requirements: The resulting (approximate) 2-spinon dynamic structure factor $S_{zz}^{(a)}(q, \omega) = M^{(a)}(q, \omega)D(q, \omega)$ must produce, for $q = \pi$, the correct infrared exponent.^{11,12} Furthermore, it must produce the correct q -dependence of the known first frequency moment,^{8,13}

$$K_1(q) \equiv \int_0^\infty \frac{d\omega}{2\pi} \omega S_{zz}(q, \omega) = -\frac{2E_G}{3N}(1 - \cos q), \quad (2.2)$$

where $E_G = -N(\ln 2 - 1/4)$ is the ground-state energy,² and, via the sum rule

$$\chi(q) \equiv \frac{1}{\pi} \int_0^\infty \frac{d\omega}{\omega} S_{zz}(q, \omega), \quad (2.3)$$

the correct value for the direct susceptibility:^{4,5} $\chi(0) = 1/\pi^2$. The resulting approximate expression,¹⁴

$$S_{zz}^{(a)}(q, \omega) = \frac{\Theta(\omega - \omega_L(q))\Theta(\omega_U(q) - \omega)}{\sqrt{\omega^2 - \omega_L^2(q)}}, \quad (2.4)$$

for the 2-spinon dynamic structure factor has been used quite frequently for the interpretation of inelastic neutron scattering measurements on a number of quasi-1D antiferromagnets at low temperature,⁷ and for comparisons with the results of various computational studies.¹⁵⁻¹⁷

It is interesting to note in this context that the exact dynamic structure factor $S_{zz}(q, \omega)$ of the Haldane-Shastry model has a structure very similar to (2.4).¹⁸ In that model, as in the XX model, all the spectral weight of $S_{zz}(q, \omega)$ is carried by the 2-spinon excitations.

III. EXACT TRANSITION RATES

A detailed assessment of the merits and limitations of the result (2.4) has become possible only recently through a remarkable new development. By approaches based on the concept of infinite-dimensional symmetries which had been developed in the context of string theory, conformal field theory, and quantum groups¹⁹ Bougourzi, Couture, and Kacir²⁰ were able to derive the exact expression for the 2-spinon transition-rate function in the form²¹

$$M(q, \omega) = \frac{1}{2} e^{-I(t)} \quad (3.1)$$

where $t = 2(\beta_1 - \beta_2)/\pi$ and

$$I(t) = \int_0^\infty dx \frac{\cosh(2x) \cos(xt) - 1}{x \sinh(2x) \cosh x} e^{-x}, \quad (3.2)$$

$$\omega = \frac{\pi}{2 \cosh \beta_1} + \frac{\pi}{2 \cosh \beta_2}, \quad (3.3a)$$

$$q = -\cot^{-1}(\sinh \beta_1) - \cot^{-1}(\sinh \beta_2). \quad (3.3b)$$

By solving Eqs. (3.3) we can express the auxiliary variable t as a function of the two physical variables q, ω :

$$t = \frac{4}{\pi} \cosh^{-1} \sqrt{\frac{\omega_U^2(q) - \omega_L^2(q)}{\omega^2 - \omega_L^2(q)}}. \quad (3.4)$$

For the numerical evaluation of (3.1) we separate the singular part from the integral (3.2):

$$I(t) = -I_0 - \ln \left(t \sinh^2 \frac{\pi t}{4} \right) + h(t), \quad (3.5)$$

where

$$h(t) = \text{Ci}(t) + f_1(t) - f_2(t), \quad (3.6a)$$

$$f_1(t) = \int_1^\infty \frac{dx \cos(xt)}{x \cosh^2 x}, \quad f_2(t) = \int_0^1 \frac{dx \cos(xt)}{x \coth^2 x}, \quad (3.6b)$$

$$I_0 = \gamma + f_1(0) - f_2(0) = 0.3677103\dots \quad (3.6c)$$

A series expansion of $s(t) \equiv [\ln t + C - h(t)]/2$,

$$s(t) = \int_0^\infty dx \frac{\sin^2(xt/2)}{x \cosh^2 x} = \sum_{m=1}^\infty (-1)^m m \ln \left(1 + \frac{t^2}{4m^2} \right),$$

$$C \equiv e^{I_0}/2 = 0.72221\dots, \quad (3.7)$$

brings (3.1) with t from (3.4) into closed form:

$$M(q, \omega) = Ct \sinh \left(\frac{\pi t}{4} \right) \times \prod_{m=1}^\infty \frac{\{1 + [t/(4m-2)]^2\}^{2m-1}}{\{1 + [t/4m]^2\}^{2m}}. \quad (3.8)$$

The exact 2-spinon part of $S_{zz}(q, \omega)$, i.e. the function (1.7) with the density of states (1.5) and the transition-rate function (3.1) evaluated numerically via (3.5) with (3.4) is plotted in Fig. 1(a). For comparison, the approximate result (2.4) is shown in Fig. 1(b). The two results look very similar, yet there are subtle differences, which may not matter for most experimental comparisons but

are important for comparisons with other theoretical results.

Both expressions diverge at the lower spectral boundary $\omega_L(q)$. At the upper boundary $\omega_U(q)$, $S_{zz}^{(a)}(q, \omega)$ has discontinuity, whereas $S_{zz}^{(2)}(q, \omega)$ approaches zero continuously over a rounded shoulder.

The structure of the exact transition rate function (3.1) lends itself naturally to be factorized into the approximate function (2.1) and a correction which accounts for the modified singularities at the boundaries of the 2-spinon continuum:

$$M(q, \omega) = M^{(a)}(q, \omega) \sqrt{Ct/2} e^{h(t)/2}. \quad (3.9)$$

IV. SINGULARITIES AT $\omega_L(q)$ AND $\omega_U(q)$

What is the precise nature of the leading singularity in the transition-rate function $M(q, \omega)$ and in the 2-spinon dynamic structure factor $S_{zz}^{(2)}(q, \omega)$ at the spectral boundaries $\omega_U(q)$ and $\omega_L(q)$, and how do these singularities compare with those of the approximate results $S_{zz}^{(a)}(q, \omega)$ and $M^{(a)}(q, \omega)$? The answer is obtained by inserting (3.5) into (3.1), evaluating the leading term for $t \rightarrow 0$ and $t \rightarrow \infty$, respectively, and inserting (3.4) expanded accordingly.

At $\omega_U(q)$ the transition-rate function is thus found to approach zero linearly,

$$M(q, \omega) \xrightarrow{\omega \rightarrow \omega_U} \frac{8C}{\pi} \frac{\omega_U(q)}{\omega_U^2(q) - \omega_L^2(q)} [\omega_U(q) - \omega], \quad (4.1)$$

which implies that the 2-spinon dynamic structure factor vanishes in a square-root cusp:

$$S_{zz}^{(2)}(q, \omega) \xrightarrow{\omega \rightarrow \omega_U} \frac{8C}{\pi} \frac{\sqrt{2\omega_U(q)}}{\omega_U^2(q) - \omega_L^2(q)} \sqrt{\omega_U(q) - \omega}. \quad (4.2)$$

$M^{(a)}(q, \omega)$ vanishes more slowly, $\sim [\omega_U(q) - \omega]^{1/2}$, implying that $S_{zz}^{(a)}(q, \omega)$ drops to zero abruptly.

At $\omega_L(q)$ we find a square-root divergence (for $q \neq \pi$) in both the exact and the approximate transition-rate functions, but in the former this power-law singularity is accompanied by a logarithmic correction:

$$M(q, \omega) \xrightarrow{\omega \rightarrow \omega_L} \frac{\sqrt{C/2}}{\pi} \sqrt{\frac{\omega_U^2(q) - \omega_L^2(q)}{\omega_L(q)}} \times \frac{1}{\sqrt{\omega - \omega_L(q)}} \sqrt{\ln \frac{1}{\omega - \omega_L(q)}}. \quad (4.3)$$

Since the 2-spinon density of states is a step function near $\omega_L(q)$, only the prefactor changes in $S_{zz}^{(2)}(q, \omega)$:

$$S_{zz}^{(2)}(q, \omega) \xrightarrow{\omega \rightarrow \omega_L} \frac{M(q, \omega)}{\sqrt{\omega^2(q) - \omega_L^2(q)}}. \quad (4.4)$$

For $q \rightarrow \pi$ the singularity at $\omega_L(q)$ turns into a much stronger infrared singularity:

$$M(\pi, \omega) \xrightarrow{\omega \rightarrow 0} \sqrt{2\pi C} \frac{1}{\omega} \sqrt{\ln \frac{1}{\omega}}, \quad (4.5)$$

$$S_{zz}^{(2)}(\pi, \omega) \xrightarrow{\omega \rightarrow 0} \sqrt{\frac{2C}{\pi}} \frac{1}{\omega} \sqrt{\ln \frac{1}{\omega}}. \quad (4.6)$$

V. SPIN AUTOCORRELATION FUNCTION

A quantity of some interest in various experimental and theoretical contexts is the frequency-dependent spin autocorrelation function

$$\Phi_{zz}(\omega) \equiv \int_{-\infty}^{+\infty} dt e^{-i\omega t} \langle S_I^z(t) S_I^z \rangle. \quad (5.1)$$

The 2-spinon contribution to $\Phi_{zz}(\omega)$,

$$\Phi_{zz}^{(2)}(\omega) \equiv \frac{1}{\pi} \int_0^\pi dq S_{zz}^{(2)}(q, \omega), \quad (5.2)$$

is a piecewise smooth function over the range of 2-spinon energies $0 < \omega < \pi$ and has singularities at $\omega = 0, \pi/2, \pi$. The approximate 2-spinon autocorrelation function inferred from (2.4) can be evaluated in terms of elliptic integrals. It has a step discontinuity at $\omega = 0$,

$$\Phi_{zz}^{(a)}(\omega) \xrightarrow{\omega \rightarrow 0} \frac{1}{\pi} + O(\omega), \quad (5.3)$$

a logarithmic divergence at $\omega = \pi/2$,

$$\Phi_{zz}^{(a)}(\omega) \xrightarrow{\omega \rightarrow \pi/2} \propto \ln \frac{1}{|\pi/2 - \omega|}, \quad (5.4)$$

and a square-root cusp at $\omega = \pi$,

$$\Phi_{zz}^{(a)}(\omega) \xrightarrow{\omega \rightarrow \pi} \propto \sqrt{\pi - \omega}. \quad (5.5)$$

The exact 2-spinon expression has logarithmic divergences at $\omega = 0, \pi/2$, and a linear cusp at $\omega = \pi$:

$$\Phi_{zz}^{(2)}(\omega) \xrightarrow{\omega \rightarrow 0} \propto \ln \frac{1}{\omega}. \quad (5.6)$$

$$\Phi_{zz}^{(2)}(\omega) \xrightarrow{\omega \rightarrow \pi/2} \propto \left(\ln \frac{1}{|\pi/2 - \omega|} \right)^{3/2}, \quad (5.7)$$

$$\Phi_{zz}^{(2)}(\omega) \xrightarrow{\omega \rightarrow \pi} \propto (\pi - \omega) \quad (5.8)$$

The functions $\Phi_{zz}^{(2)}(\omega)$ and $\Phi_{zz}^{(a)}(\omega)$ are plotted in Fig. 2.

VI. SUM RULES

How important is the 2-spinon contribution to $S_{zz}(q, \omega)$ in relation to that of other excited states? The key to the answer is provided by sum rules, such as the first frequency moment (2.2), which is known for all q , or the susceptibility (2.3), which is known for $q = 0$ only, or the integrated intensity (static structure factor),

$$I(q) \equiv \int_0^\infty \frac{d\omega}{2\pi} S_{zz}(q, \omega), \quad (6.1)$$

of which we know the grand total:

$$I_T = \frac{1}{\pi} \int_0^\pi dq I(q) = \langle (S_i^z)^2 \rangle = \frac{1}{4}. \quad (6.2)$$

The exact 2-spinon contribution to the n^{th} frequency moment of $S_{zz}(q, \omega)$,

$$K_n(q) \equiv \int_0^\infty \frac{d\omega}{2\pi} \omega^n S_{zz}(q, \omega), \quad (6.3)$$

as obtained from (1.7) with (1.5) and (3.1) can be brought into the form

$$K_n^{(2)}(q) = \frac{2C}{\pi^3} [\omega_U(q)]^{n+1} k_n(q), \quad (6.4)$$

where

$$k_n(q) = \int_0^\infty dx \frac{x \sinh x}{\cosh^2 x} \left(1 - \sin^2 \frac{q}{2} \tanh^2 x\right)^{\frac{n-1}{2}} e^{-s(4x/\pi)}. \quad (6.5)$$

For $n = 2m + 1 = 1, 3, \dots$ this expression reduces to a polynomial in $\cos q$,

$$K_{2m+1}^{(2)}(q) = \frac{C}{\pi} \left(\frac{\pi^2}{2}\right)^m \sum_{l=0}^m \binom{m}{l} \frac{(-1)^l}{2^l} \kappa_l (1 - \cos q)^{m+1+l}, \quad (6.6a)$$

$$\kappa_l \equiv \int_0^\infty dx \frac{x (\tanh x)^{2l+1}}{\cosh x} e^{-s(4x/\pi)}. \quad (6.6b)$$

The exact sum rules for $K_{2m+1}(q)$ were shown to have precisely this general structure,^{22,23} which, incidentally, is also reproduced by the frequency moments $K_{2m+1}^{(a)}(q)$ of $S_{zz}^{(a)}(q, \omega)$. However, the exact coefficients of the polynomial are only known for $m = 0$. Comparison of

$$K_1^{(2)}(q) = \frac{C}{\pi} \kappa_0 (1 - \cos q), \quad \kappa_0 = 0.9163\dots, \quad (6.7)$$

with (2.2) provides one way of measuring the relative spectral weight of the 2-spinon excitations:

$$\frac{K_1^{(2)}(q)}{K_1(q)} = 0.7130\dots \quad (6.8)$$

A somewhat larger share of spectral weight, $K_1^{(a)}(q)/K_1(q) = 0.8462\dots$, is accounted for by $S_{zz}^{(a)}(q, \omega)$.

A different way of measuring the relative 2-spinon spectral weight is provided by the static structure factor (6.1). Here, the missing spectral weight of higher-lying excitations is weighted less heavily.

The exact 2-spinon static structure factor $I^{(2)}(q) = K_0^{(2)}(q)$ taken from (6.4) and integrated over q yields the total 2-spinon intensity

$$I_T^{(2)} = \frac{4C}{\pi^3} \int_0^\infty dx \frac{x^2}{\cosh x} e^{-s(4x/\pi)} \simeq 0.7289 I_T. \quad (6.9)$$

The total intensity of $S_{zz}^{(a)}(q, \omega)$ is⁸ $I_T^{(a)} \simeq 0.7424 I_T$.

The observation that $S_{zz}^{(a)}(q, \omega)$ overestimates the total 2-spinon intensity by a smaller fraction, $I_T^{(a)}/I_T^{(2)} \simeq 1.0185$, than the first frequency moment of the 2-spinon spectral weight, $K_1^{(a)}(q)/K_1^{(2)}(q) \simeq 1.1868$, is consistent with the observation made previously that it predicts too much spectral weight near $\omega_U(q)$ and too little near $\omega_L(q)$.

At small q , where the 2-spinon continuum is very narrow, all frequency moments of $S_{zz}^{(2)}(q, \omega)$ and $S_{zz}^{(a)}(q, \omega)$ have exactly the same ratio

$$\frac{K_n^{(a)}(q)}{K_n^{(2)}(q)} \xrightarrow{q \rightarrow 0} \frac{4C}{\pi} \kappa_0 = 0.8426\dots \quad (6.10)$$

The implications of the frequency moments $K_0^{(2)}(q)$ and $K_{-1}^{(2)}(q)$ for the singularities of the static structure factor and the static susceptibility, respectively, will be discussed later.

VII. FINITE-CHAIN RESULTS

To what extent and accuracy can the spectral-weight distribution of $S_{zz}(q, \omega)$ be reconstructed from (1.6) on the basis of finite-chain data for excitation energies ω_λ and transition rates M_λ ? In a generic situation, the chances for success may be remote. Convergence of the finite- N data for (1.6) toward the infinite- N spectral density may only exist in an average sense, such as can be realized, at least in principle, by a histogram representation of (1.6), but hardly in practice given the very coarse-grained spectral-weight distribution even in the largest systems that can be handled computationally.

Among the ever growing collection of Bethe-ansatz solvable models, there exist numerous situations where

the spectral density of interest is dominated by a specific class of excitations that can be identified in terms of Bethe quantum numbers. When the dynamically dominant class of excitations consists of a two-parameter continuum, as is frequently the case, the task of reconstructing that spectral density from finite- N data with reasonable accuracy may be perfectly within the reach of state-of-the-art computational applications.

In the case at hand, the 2-spinon excitation energies ω_λ can be evaluated for finite chains over a wide range of N and then again for infinite N , all via Bethe ansatz. The finite- N transition rates M_λ can be evaluated directly from the Bethe-ansatz wave function for the ground state and the 2-spinon states up to $N = 16$ and indirectly from the finite- N ground-state wave function via the recursion method¹⁷ up to $N = 28$.

The crucial point for the reconstruction of the 2-spinon part of the dynamic structure factor $S_{zz}(q, \omega)$ is that it factorizes into two smooth functions: the density of states $D(q, \omega)$, which can be determined exactly via Bethe ansatz, and the transition rate function $M(q, \omega)$, toward which the finite- N transition rates seem to converge in the following sense: pick any sequence of finite- N 2-spinon states with energies $\omega_\lambda(N)$ and wave numbers $q_\lambda(N)$ converging toward (q, ω) as $N \rightarrow \infty$. Then the associated scaled transition rates $NM_\lambda(N)$ converge toward the exact transition rate function $M(q, \omega)$.

In the main plot of Fig. 3 we show the transition rate functions $M(\pi, \omega)$ (exact, solid line) and $M^{(a)}(\pi, \omega)$ (approximate, dashed line) along with scaled finite- N transition rates NM_λ for $N = 6, 8, \dots, 28$. The downward deviation of $M^{(a)}(\pi, \omega)$ from $M(\pi, \omega)$ at low frequencies is due to the lacking logarithmic corrections in the infrared divergence and the upward deviation at high frequencies due to the different cusp singularity at $\omega_U(\pi)$.

All finite- N data points fall close to the solid line. Their deviations from that line have an irregular appearance at first sight. This is attributable to the fact that an increasing number of spectral contributions from systems with increasing N are distributed over a fixed frequency interval. However, when we focus on the lowest-lying excitation, for example, we see that the data points move away from the dashed line toward the solid line. The uniform convergence of this particular sequence of data points is best observable in the representation of the inset on the left of Fig. 3.

The region near $\omega_U(\pi)$ is shown magnified in the inset on the right. Here the finite- N data converge in a much more complicated pattern. Nevertheless, the trend is clearly toward the linear behavior of the solid line and away from the square-root behavior of the dashed line.

The corresponding results for $q = \pi/2$ are depicted in Fig. 4. Here the highest 2-spinon excitation for $N = 28$, which we were unable to compute with sufficient accuracy via the recursion method, is not included. Even with the few finite-chain data points available in this case, the finite-size scaling behavior of the transition rates M_λ and their convergence toward the exact transition-rate

function is again convincingly determined.

Given the exact asymptotic finite-size gap of the lowest 2-spinon excitation at $q = \pi$,²⁴

$$\omega_1 \xrightarrow{N \rightarrow \infty} \frac{\alpha}{N}, \quad \alpha = \frac{\pi^2}{2}, \quad (7.1)$$

and the exact infrared divergence (4.6) of $S_{zz}^{(2)}(q, \omega)$, it is possible to determine, under standard scaling assumptions, the leading N -dependence of the integrated intensity at $q = \pi$,

$$I(\pi, N) \xrightarrow{N \rightarrow \infty} \frac{m_0}{2\pi} (\ln N)^{3/2} \quad (7.2)$$

with $m_0 = \sqrt{2C/\pi}$. The exact coefficient, $m_0/2\pi = 0.1079\dots$, is significantly higher than the value 0.09052 predicted in a recent DMRG study.²⁵ The leading singularity of the integrated intensity for $N = \infty$, $q \rightarrow \pi$ is then predicted to be of the form

$$I(q, \infty) \xrightarrow{q \rightarrow \pi} \frac{m_0}{2\pi} \left[-\ln \left(1 - \frac{q}{\pi} \right) \right]^{3/2}, \quad (7.3)$$

which is consistent with the exactly known leading asymptotic term of the static spin correlation function²⁶ $\langle S_i^z S_{i+n}^z \rangle \sim (-1)^n n^{-1} (\ln n)^{1/2} / n$.

The corresponding leading terms for the static susceptibility read:

$$\chi(\pi, N) \xrightarrow{N \rightarrow \infty} \frac{m_0}{\pi\alpha} N \sqrt{N}, \quad (7.4)$$

$$\chi(q, \infty) \xrightarrow{q \rightarrow \pi} \propto \frac{\sqrt{-\ln(\pi - q)}}{\pi - q}. \quad (7.5)$$

ACKNOWLEDGMENTS

The work at URI was supported by NSF Grant DMR-93-12252, and by the Max Kade Foundation. The work at SUNYSB was supported by NSF Grant PHY-93-09888. A.H.B. would like to thank M. Couture for encouragements and stimulating discussions. Access to the computing facilities at the national Center for Supercomputing Applications, University of Illinois at Urbana-Champaign is gratefully acknowledged.

¹ H. Bethe, Z. Phys. **71**, 205 (1931).

² L. Hulthén, Arkiv Mat. Astron. Fysik A11 **26**, 1 (1938).

³ J. des Cloizeaux and J.J. Pearson, Phys. Rev. **128**, 2131 (1962).

⁴ R.B. Griffiths, Phys. Rev. **133**, A768 (1964).

⁵ C.N. Yang and C.P. Yang, Phys. Rev. **150**, 321 (1966); **150**, 327 (1966); **151**, 258 (1966).

- ⁶ M. Gaudin, Phys. Rev. Lett. **26**, 1301 (1971); M. Takahashi, Prog. Theor. Phys. **46**, 401 (1971).
- ⁷ S.E. Nagler *et al.*, Phys. Rev. B **44**, 12361 (1991); D.A. Tennant, T.G. Perring, R.A. Cowley, and S.E. Nagler, Phys. Rev. Lett. **70**, 4003 (1993); D.C. Dender *et al.*, Phys. Rev. B **53**, 2583 (1996).
- ⁸ G. Müller, H. Thomas, H. Beck, and J.C. Bonner, Phys. Rev. B **24**, 1429 (1981).
- ⁹ T. Niemeijer, Physica **36**, 377 (1966).
- ¹⁰ S. Katsura, T. Horiguchi, and M. Suzuki, Physica **46**, 67 (1970).
- ¹¹ A. Luther and I. Peschel, Phys. Rev. B **12**, 3908 (1975).
- ¹² The logarithmic corrections to the $\sim \omega^{-1}$ singularity were not known at the time.
- ¹³ P.C. Hohenberg and W.F. Brinkman, Phys. Rev. B **10**, 128 (1974).
- ¹⁴ Alternative requirements considered in Ref. 8 yield prefactors in (8) which are slightly greater than one.
- ¹⁵ S. Haas, J. Riera, and E. Dagotto, Phys. Rev. B **48**, 3281 (1993).
- ¹⁶ K. Hallberg, Phys. Rev. B **52**, R9827 (1995).
- ¹⁷ A. Fledderjohann, M. Karbach, K.-H. Mütter, and P. Wielath, J. Phys.: Condens. Matter **7**, 8993 (1995).
- ¹⁸ F.D.M. Haldane and M.R. Zirnbauer, Phys. Rev. Lett. **71**, 4055 (1993).
- ¹⁹ M. Jimbo and T. Miwa, *Algebraic Analysis of Solvable Lattice Models*, (American Mathematical Society, CBMS, 1995).
- ²⁰ A.H. Bougourzi, M. Couture, and M. Kacir, Preprint ITP-SB-96-21, Stony Brook.
- ²¹ We have found and corrected a discrepancy in chapter 10.4 of Ref. 19, which affects the constant prefactor in (3.1).
- ²² A. Fledderjohann, M. Karbach, and K.-H. Mütter, Phys. Rev. B **53**, 11543 (1996).
- ²³ G. Müller, Phys. Rev. B **26**, 1311 (1982).
- ²⁴ F. Woynarovich and H.-P. Ecker, J. Phys. A: Math. Gen. **20**, L97 (1987).
- ²⁵ K. Hallberg, P. Horsch, and G. Martínez, Phys. Rev. B **52**, R719 (1995).
- ²⁶ R.R.P. Singh, M.E. Fisher, and R. Shankar, Phys. Rev. B **39**, 2562 (1989).

FIG. 1. (a) Exact and (b) approximate 2-spinon dynamic structure factor. Both expressions are nonzero only in the shaded region of the (q, ω) -plane bounded by $\omega_L(q)$ and $\omega_U(q)$.

FIG. 2. Two-spinon part of the frequency-dependent spin autocorrelation function. The solid line represents the exact result $\Phi_{zz}^{(2)}(\omega)$ and the dashed line the approximate result $\Phi_{zz}^a(\omega)$.

FIG. 3. Two-spinon transition-rate function at $q = \pi$. The solid line represents the exact result $M(q, \omega)$ and the dashed line the approximate result $M^{(a)}(q, \omega)$. Also shown are scaled finite-chain transition rates NM_λ for all 2-spinon excitations at $q = \pi$ of systems with $N = 6, 8, \dots, 16, 28$ spins, and for lowest 2-spinon excitations also of systems with $N = 18, 20, \dots, 26$. The low-frequency and high-frequency parts are shown again in the insets with transformed scales on both axes.

FIG. 4. Two-spinon transition-rate function at $q = \pi/2$. The solid line represents the exact result $M(q, \omega)$ and the dashed line the approximate result $M^{(a)}(q, \omega)$. Also shown are scaled finite-chain transition rates NM_λ for all 2-spinon excitations at $q = \pi$ of systems with $N = 8, 12, 16, 28$ spins. The low-frequency and high-frequency parts are shown again in the insets with transformed scales on both axes.